NJC

Accepted Manuscript

This is an *Accepted Manuscript*, which has been through the Royal Society of Chemistry peer review process and has been accepted for publication.

Accepted Manuscripts are published online shortly after acceptance, before technical editing, formatting and proof reading. Using this free service, authors can make their results available to the community, in citable form, before we publish the edited article. We will replace this *Accepted Manuscript* with the edited and formatted *Advance Article* as soon as it is available.

You can find more information about *Accepted Manuscripts* in the Information for Authors.

Please note that technical editing may introduce minor changes to the text and/or graphics, which may alter content. The journal's standard Terms & Conditions and the Ethical guidelines still apply. In no event shall the Royal Society of Chemistry be held responsible for any errors or omissions in this *Accepted Manuscript* or any consequences arising from the use of any information it contains.

ROYAL SOCIETY OF CHEMISTRY

www.rsc.org/njc

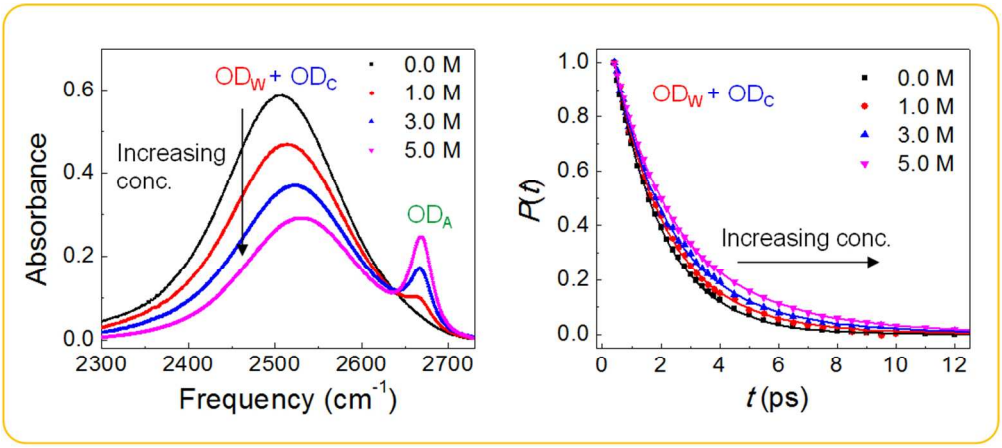

298x132mm (96 x 96 DPI)

Vibrational Probing of the Hydrogen-Bond Structure and Dynamics of Water in Aqueous $NaPF_6$ Solutions

Chiho Lee,[1‡] Dayoung Nam,[1‡] and Sungnam Park[1,2*]

[1]Department of Chemistry, Korea University, Seoul 136-701, Korea.

[2]Multidimensional Spectroscopy Laboratory, Korea Basic Science Institute, Seoul 136-713, Korea.

[*]Authors to whom correspondence should be addressed.

Email addresses: spark8@korea.ac.kr

[‡]The authors are equally contributed.

Abstract

Direct measurements of the individual dynamics of water in bulk and ionic hydration shells in aqueous ionic solutions are quite experimentally challenging because the different subsets of water in bulk and ionic hydration shells are not spectrally well-resolved in most aqueous ionic solutions. In contrast, the different subsets of water in bulk, cationic hydration shell, and anionic hydration shell in aqueous $NaPF_6$ solutions were found to be spectrally well distinct. Such spectral features allowed us to study the individual dynamics of the different subsets of water in aqueous $NaPF_6$ solutions. In this work, we studied the hydrogen-bond (H-bond) structure and dynamics of water in aqueous $NaPF_6$ solutions at different $NaPF_6$ concentrations by FTIR, Raman, and IR pump-probe spectroscopy. Three different subsets of water in bulk, cationic hydration shell, and anionic hydration shell were found to have their own characteristic hydroxyl stretch peaks (eigen spectra) in FTIR and Raman spectra and have unique vibrational lifetimes independent of $NaPF_6$ concentration. However, the orientational relaxation dynamics, $r(t)$, were not able to be separately measured for three different subsets of water. The overall orientational relaxation times were found to be linearly dependent on the solution viscosity and were reasonably well described by the Debye-Stokes-Einstein equation. Finally, the frequency-dependent transition dipole moments of the hydroxyl (−OD) stretch vibration obtained in neat water and aqueous 3.0 M $NaPF_6$ solution were compared and found to be dependent on the nature of H-bonds.

I. Introduction

Hydrogen-bond (H-bond) structure and dynamics of water in aqueous ionic solutions are strongly influenced by dissolved ions.[1-9] The properties of aqueous ionic solutions deviate substantially from those of neat water because the H-bond network of water is substantially perturbed by dissolved ions, especially at high ionic concentrations.[10] When water molecules form hydration shells around dissolved ions in aqueous ionic solutions, the dynamic properties of water in ionic hydration shells should be quite different from those in bulk. However, there has been an experimental difficulty in directly measuring the dynamics of water in ionic hydration shells. Using femtosecond IR spectroscopy, the dynamics of water in aqueous ionic solutions have been extensively studied by directly probing the hydroxyl stretch (-OD or -OH) of HOD in an isotopically diluted water (i.e., HOD in H_2O or HOD in D_2O). The hydroxyl stretch bands in aqueous solutions are normally very broad ($\Delta\omega$ = ~160 cm^{-1} in FWHM) due to an inhomogeneous distribution of H-bond configurations. In most aqueous ionic solutions, the hydroxyl stretch bands of water molecules in bulk and ionic (i.e., cationic and anionic) hydration shells are significantly overlapped and are not spectrally well-resolved. Such broad spectral features make it difficult to directly investigate the different subsets of water in bulk and ionic hydration shells. Therefore, what has been measured with aqueous ionic solutions is the weighted-averaged dynamics of water in bulk and ionic hydration shells. Direct measurements of the dynamics of water in ionic hydration shells are of importance to better understand the properties of aqueous ionic solutions in the first place and the behaviors of water molecules at many different charged interfaces, such as reverse micelles,[11-15] protein surfaces, and so on.

The PF_6^- ion has been known for a long time to have its peculiar properties in water and electrolyte solutions. The electrolyte solutions with PF_6^- ions are technically important due to their applications in Li^+ ion secondary batteries[16, 17] and room temperature ionic

liquids (RTILs).[18-21] Aqueous PF_6^- solutions are found to be a good model system to study the H-bond structure and dynamics of water because the water molecules in aqueous PF_6^- solutions can be spectrally decomposed into three different subsets of water, i.e., water molecules in bulk (OD_W) and cationic and anionic hydration shells (OD_C and OD_A, respectively) in FTIR and Raman spectra. In fact, PF_6^- ions in aqueous solutions were used for the peak separations of water in static IR or Raman studies.[22-24] These spectral features can provide an opportunity to study the individual dynamics of water in two H-bond configurations and further in cationic and anionic hydration shells in aqueous PF_6^- solutions. Recently, we have investigated the H-bond exchange dynamics occurring in aqueous 5.0 M $NaPF_6$ solution by two-dimensional infrared spectroscopy being able to directly determine the H-bond exchange time constants.[25] More recently, we have reported a detailed study of the temperature dependence of linear FTIR spectrum, vibrational population decay, and orientational relaxation dynamics of water in aqueous 5.0 M $NaPF_6$ solution.[26]

In the present work, we studied the concentration-dependent H-bond structure and dynamics of water in aqueous $NaPF_6$ solutions by FTIR, Raman, and IR pump-probe experiments. First of all, the hydroxyl (-OD) stretch band of HOD in FTIR and Raman spectra measured at different $NaPF_6$ concentrations were found to be decomposed into the three peaks corresponding to the eigen spectra of three different subsets (OD_W, OD_C, and OD_A) of water in aqueous $NaPF_6$ solutions. Second, vibrational population relaxation and orientational relaxation dynamics of water in three different subsets were investigated at different $NaPF_6$ concentrations. Finally, the frequency-dependent transition dipole moment of water in neat water and 3.0 M $NaPF_6$ solution was determined by comparing the FTIR and Raman spectra.

II. Experimental methods

A. Sample preparation

Deionized water (H_2O) from Millipore and D_2O (99.9% purity, Sigma Aldrich) were used to prepare the isotopically diluted water (8% HOD in H_2O) by mixing D_2O and H_2O with 4:96 volume ratio. For our experiments, 1.0, 3.0, and 5.0 M $NaPF_6$ solutions were prepared by directly dissolving appropriate amounts of $NaPF_6$ (98% purity, Sigma Aldrich) salt in isotopically diluted water. In addition, the reference solutions with the same molar concentrations in H_2O were prepared for the background correction. For FTIR and IR pump-probe experiments, all the sample solutions were housed in home-made IR cells with two 3 mm thick CaF_2 windows and a 25 μm thick Teflon spacer. The solution viscosity was measured by using the Ostwald viscometer at 22 °C. The time of flow of the solution between two marked lines in the Ostwald viscometer was measured. For a given solution, the experiments were repeated more than three times and the average lapse time was used to determine the solution viscosity by comparing it with the time required for pure water (η_0=0.955 cP at 22 °C).

B. Fourier transform infrared (FTIR) spectroscopy

FTIR spectra of all the sample solutions were measured by using a Varian 640-IR spectrometer in the range of 400-4000 cm^{-1} with a 1 cm^{-1} resolution. The sample spectra were background-corrected by subtracting the spectra of the reference solutions from those of the sample solutions. All FTIR spectra were measured at 22 °C.

C. Raman spectroscopy

Our Raman experimental setup consists of a 100 mW 532 nm green laser (MGL-III-532, Changchun New Industries Optoelectronics Tech. Co., Ltd) and a monochromator (Shamrock

SR-303i-B, Andor Technology) coupled with a CCD camera (iDus DU-401A-BV, Andor Technology). A Raman edge filter (Edmund optics) was placed in front of the monochromator to attenuate the intense Rayleigh scattering. Raman spectra of the samples were measured down to ~100 cm^{-1} with the frequency resolution of ~1.7 cm^{-1}. The sample solutions were contained in a 5×5 mm quartz cell (Starna Scientific Limited). Raman spectrum was also background-corrected by subtracting the reference spectrum from the sample spectrum. All Raman spectra were measured at 22 °C.

D. IR pump-probe spectroscopy

Our femtosecond mid-IR laser system is presented in detail elsewhere.[25, 27, 28] Briefly, a train of mid-IR pulses with ~1.5 μJ per pulse and ~260 cm^{-1} in FWHM are generated from our femtosecond mid-IR laser system and sent to the IR pump-probe experimental setup. The mid-IR pulse is split into the pump and probe beams with a 9:1 intensity ratio by a ZnSe beam splitter. The probe beam goes through a linear delay stage to control the relative time delay between the probe and pump pulses. The pump and probe beams pass through the wire grid polarizers where the polarization states are set to be 0° and 45° with respect to the normal to the optical table, respectively. These beams are focused onto the sample by a concave mirror (focal length, f.l. = 100 mm). After the sample, the probe beam is collimated by a concave mirror (f.l. = 100 mm) and pass through the analyzer wire grid polarizer on a motorized rotational stage and its polarization state is able to be controlled (0° or 90°). The probe beam is dispersed through a monochromator onto the 64-element mercury-cadmium-telluride (MCT) array detector. The parallel and perpendicular IR pump-probe signals, $S_{\parallel}(\omega_{\mathrm{pr}}, t)$ and $S_{\perp}(\omega_{\mathrm{pr}}, t)$, are measured by setting the polarization of the probe beam relative to the polarization of the pump beam, respectively.

III. Results and discussion

A. Analysis of FTIR spectrum: Three different subsets of water

Figure 1(A) displays the OD stretch band of HOD in aqueous $NaPF_6$ solutions at different $NaPF_6$ concentrations. When the $NaPF_6$ concentration is increased, the broad peak at the low frequency (~2510 cm^{-1}) becomes smaller and blue-shifted but the narrow peak at the high frequency (~2670 cm^{-1}) grows gradually. First of all, the narrow peak at the high frequency comes from the HOD molecules that are H-bonded to PF_6^- ions while the broad peak results from water molecules in bulk and hydration shells of Na^+ ions. By making an assumption that there exist three different subsets of water, i.e., water molecules in bulk (OD_W), cationic hydration shell (OD_C), and anionic hydration shell (OD_A) in aqueous $NaPF_6$ solutions, the OD stretch band in the FTIR spectrum, $S(\omega)$, at a given concentration is represented by the sum of the following three contributions,

$$S(\omega) = \alpha \cdot S_{OD_W}(\omega) + A_1 \cdot S_{OD_C}(\omega) + A_2 \cdot S_{OD_A}(\omega) \quad (1)$$

where α is the scaling factor, $S_{OD_W}(\omega)$ is the FTIR spectrum measured at 0.0 M, $S_{OD_C}(\omega)$ and $S_{OD_A}(\omega)$ are the normalized pseudo-Voigt profiles to fit the OD_C and OD_A, respectively (for the fit parameters, see Table S1 in ESI). The first term in Eq. (1) is associated with the relative amount of spectroscopically-distinct bulk water in aqueous $NaPF_6$ solutions with $\alpha \leq 1$. Among three contributions (OD_W, OD_C, and OD_A), the OD_A is peaked separately at 2669±1 cm^{-1} while the low frequency broad peak consists of the OD_W at 2508±1 cm^{-1} and the OD_C at 2541±1 cm^{-1}. Therefore, the decomposition of the low frequency peak into the OD_W and OD_C contributions is a key analysis. By using the global fitting analysis, the OD stretch band in aqueous $NaPF_6$ solutions can be readily decomposed into three contributions. Figure 1(B) shows the OD_W, OD_C, and OD_A contributions in 3.0 M $NaPF_6$ solution. Three individual

OD peaks shown in Figure 1(B) can be thought of as the eigen spectra of the OD_W, OD_C, and OD_A contributions. The water molecules in cationic hydration shells appear at the higher frequency relative to the bulk water as shown in Figure 1(B). Figure 1(C) presents the relative areas of three OD peaks as a function of $NaPF_6$ concentration. As indicated in Figure 1(C), the amount of bulk water is gradually decreased with increasing $NaPF_6$ concentration while the amount of water molecules in cationic and anionic hydration shells is increased. Accordingly, the blue-shift of the low frequency peak in Figure 1(A) with increasing $NaPF_6$ concentration can be easily explained by the fact that more and more water molecules in bulk participate in hydration of Na^+ ions leading to the gradual blue-shift of the low frequency band.

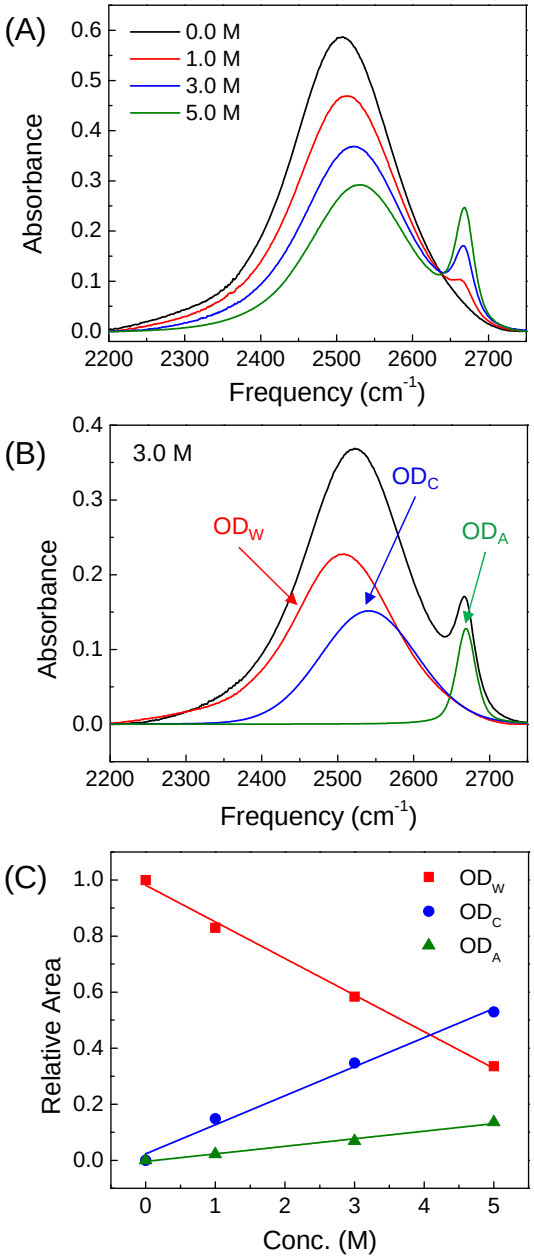

Figure 1. (A) The OD stretch band in the FTIR spectra measured with aqueous $NaPF_6$ solutions at different concentrations. (B) Decomposition of the OD stretch band into three contributions: the OD stretch band of water in bulk (OD_W, peaked at 2508 cm^{-1}), hydration shells of Na^+ ions (OD_C, peaked at 2541 cm^{-1}), and hydration shells of PF_6^- ions (OD_A, peaked at 2669 cm^{-1}). (C) Relative areas of three OD stretch peaks are plotted as a function of $NaPF_6$ concentration.

B. Quantum chemical calculations

Quantum chemical calculations were carried out to estimate the OD stretch frequency of HOD molecules in bulk and ionic hydration shells. As shown in Figure 2, ion-HOD clusters were used for the quantum chemical calculations. The density functional theory (DFT) method (B3LYP functional) with a DGDZVP basis set was used to optimize the ion-HOD clusters shown in Figures 2(A) and 2(B) and calculate the OD stretch frequency of HOD molecules in different configurations, i.e., OD_W (HO–D···OHD), OD_C (Na^+···HO–D···OHD), and OD_A (PF_6^-···D–OH).[29] The solid line in Figure 2(C) is the IR spectrum calculated from the PF_6^- and HOD cluster in Figure 2(A) and the dashed-dotted line is the IR spectrum calculated from the Na^+ and HOD cluster in Figure 2(B). As indicated by the separated areas in Figure 2(C), the OD stretch frequencies calculated from ion-HOD clusters are spectrally well distinct for different configurations. For OD_W configurations, the OD stretch frequencies, which depend on the O-O distance between two H-bonded HOD molecules, are more red-shifted for the shorter H-bonded HOD molecules. The OD stretch peaks of non-H-bonded HOD molecules (Na^+···HO–D, PF_6^-···HO–D, or H_2O···HO–D) are found to appear in the OD_A region in Figure 2(C). Quantum chemical calculations with more diverse ion-HOD clusters would give statistically more reliable IR spectrum which could be directly compared with the experimentally measured IR spectrum. Nonetheless, our simple quantum chemical calculation results with two ion-HOD clusters are qualitatively in good agreement with the decomposed spectra of the OD_W, OD_C, and OD_A.

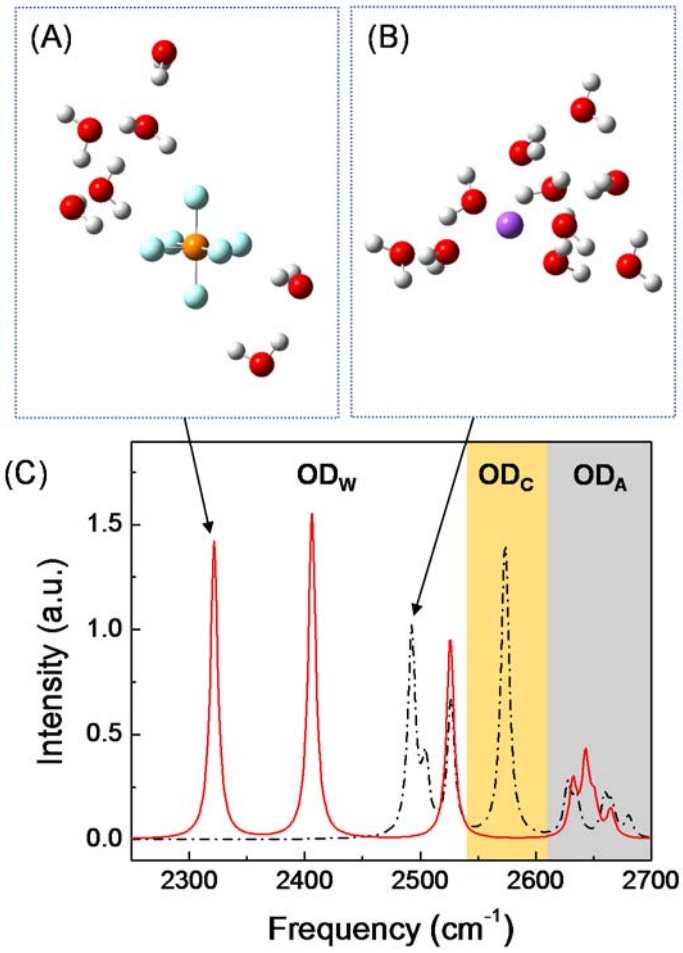

Figure 2. Quantum chemical calculations of ion-water clusters. (A) PF_6^- and HOD cluster. (B) Na^+ and HOD cluster. (C) Calculated IR spectra of OD stretch of HOD molecules in the PF_6^- and HOD cluster (solid line) and Na^+ and HOD cluster (dashed-dotted line), respectively. The calculated frequency is rescaled by a scaling factor of 0.9654.[30]

C. Dynamics of water in aqueous $NaPF_6$ solutions

Vibrational population relaxation dynamics, $P(t)$, and orientational relaxation dynamics, $r(t)$, of water in different subsets of water in aqueous $NaPF_6$ solutions were separately measured and investigated. Here, IR PP signals measured at the maximum position of the low and high frequency peaks were used to determine $P(t)$ and $r(t)$. The IR PP signals measured with

aqueous $NaPF_6$ solutions decayed to a constant offset due to the heating effect, which were taken into account to extract $P(t)$ and $r(t)$.[26, 31, 32]

C-1. Population relaxation dynamics of water

Figure 3(A) displays the population decay of the low frequency peak at different $NaPF_6$ concentrations. As discussed in the previous section, the low frequency peak consists of the OD_W and OD_C. Accordingly, the two-state model is used to determine the vibrational lifetimes of HOD in two different configurations,[31]

$$P(t) = \left(\frac{a_1}{a_1 + a_2} \right) \cdot \exp(-t / T_{1,\mathrm{OD_W}}) + \left(\frac{a_2}{a_1 + a_2} \right) \cdot \exp(-t / T_{1,\mathrm{OD_C}}) \qquad (2)$$

where the first and second terms describe the population decay of OD_W and OD_C, respectively. In this model analysis, the population decay of the low frequency peak is assumed to be represented as the sum of the population decays of the OD_W and OD_C with relative concentration ratios. Concentration-dependent $P(t)$ of the low frequency peak was fitted by the model function in Eq. (2). The fit parameters are summarized in Table 1. In Figure 3(B), the solid lines are the fit to Eq. (2) at different concentrations. As shown in Table 1 and Figure 3, $P(t)$ of the low frequency peak at different $NaPF_6$ concentrations are shown to be reasonably well described by the two-state model. It should be mentioned that the values of a_1 and a_2 obtained in this analysis are found to be almost the same with the relative areas of the OD stretch peaks in Raman spectra (See Figure S4 in ESI). In this case, the values of a_1 and a_2 should be directly associated with the relative concentrations of OD_W and OD_C in aqueous $NaPF_6$ solutions, which are directly proportional to the relative peak areas in Raman spectra. On the other hand, the relative peak areas in FTIR spectra are not the same with those in Raman spectra and the values of a_1 and a_2 due to the non-Condon effect. The vibrational lifetimes were determined to be $T_{1,\mathrm{OD_W}} = 1.7 \pm 0.1$ ps for the OD_W and

$T_{1,OD_W} = 3.7 \pm 0.3$ ps for the ODC, respectively. As the $NaPF_6$ concentration is increased, the amplitude (a_1) of the ODW decreases while the amplitude (a_2) of the ODC increases because more water molecules participate in the hydration of Na^+ ions at higher concentrations of $NaPF_6$ salt.[33, 34] In addition, the vibrational lifetime of the OD_A peak was separately determined to be $T_{1,OD_A} = 6.6 \pm 0.5$ ps at 5.0 M $NaPF_6$ solution.

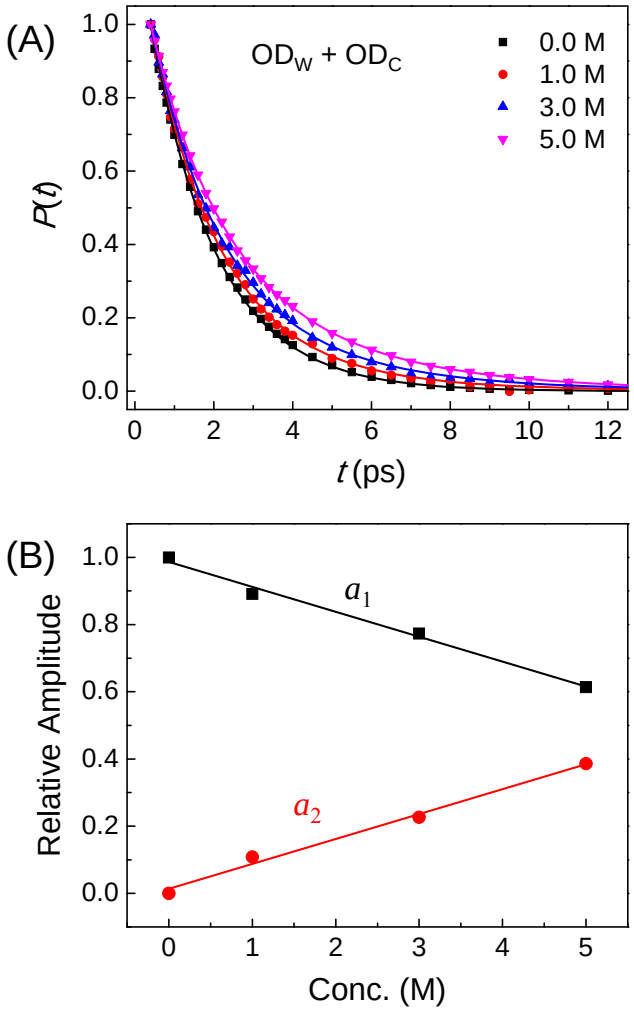

Figure 3. (A) Population decay, $P(t)$, of the low frequency peak (ODW+ODC) at ~2520 cm^{-1} at different $NaPF_6$ concentrations. (B) Amplitudes of the two-state model based on Eq. (2) are plotted as a function of $NaPF_6$ concentration.

Table 1. Parameters of the two-state model of $P(t)$ for the low frequency peak (OD_W + OD_C) at different $NaPF_6$ concentrations.

Conc. (M)	ω_{pr} (cm^{-1})	a_1	T_{1,OD_W} (ps)	a_2	T_{1,OD_C} (ps)
0.0	2508	1.00±0.03	1.7±0.1	–	–
1.0	2513	0.89±0.03	1.7±0.1	0.11±0.03	3.7±0.3
3.0	2522	0.77±0.03	1.7±0.1	0.23±0.03	3.7±0.3
5.0	2530	0.61±0.03	1.7±0.1	0.39±0.03	3.7±0.3

C-2. Orientational relaxation dynamics of water

Figure 4(A) displays the orientational anisotropy decays of the low frequency peak measured at different $NaPF_6$ concentrations. The orientational anisotropy decay, $r(t)$, is given by $r(t) = 0.4C_{or}(t)$ where $C_{or}(t)$ is the orientational correlation function and is represented by the second-order Legendre polynomial of the transition dipole correlation function, $C_{or}(t) = \langle P_2[\mu(t) \cdot \mu(0)] \rangle$. Therefore, $r(t)$ decays from the initial value of 0.4 at t=0 ps. However, the amplitudes of the orientational anisotropy decays at t=0 ps are less than 0.4 in Figure 4(A) because the initial inertial orientational relaxation of HOD molecules is not fully resolved in the measurements. The orientational anisotropy decay in Figure 4 is fitted by either a mono- or bi-exponential function. Exponential fit results are summarized in Table 2. It is found that $r(t)$ measured at 0.0, 1.0, and 3.0 M are sufficiently well fit by a mono-exponential function, $r(t) = b_1 \exp(-t/\tau_{or1})$, whereas $r(t)$ measured at 5.0 M is better fit by a biexponential function, i.e., $r(t) = b_1 \exp(-t/\tau_{or1}) + b_2 \exp(-t/\tau_{or2})$. The biexponential behavior of the orientational anisotropy decay is often described by the wobbling-in-a-cone model where the short time component of the orientational anisotropy decay results from a restricted orientational diffusion of HOD molecule due to a relatively strong intermolecular

interaction while the long time component is associated with the full diffusive orientational relaxation that is accompanied by overcoming the intermolecular interaction.[28, 35, 36] It should be noted that $r(t)$ decays slightly faster at 1.0 M than 0.0 M as shown in Table 2 and Figure 4(A). This observation results from the concentration-dependent viscosity, $\eta(c)$, of aqueous $NaPF_6$ solutions, which will be discussed later in more detail.

Table 2. Exponential fit to the orientational anisotropy decay, $r(t)$, of the low frequency peak (OD_W + OD_C).

Conc. (M)	ω_{pr} (cm^{-1})	η (cP)	b_1	τ_{or1} (ps)	b_2	τ_{or2} (ps)
0.0	2508±1	1.00±0.01	0.34±0.02	2.5±0.14	–	–
1.0	2513±1	0.98±0.01	0.33±0.02	2.4±0.24	–	–
3.0	2522±1	1.15±0.01	0.33±0.02	3.2±0.13	–	–
5.0	2530±1	1.67±0.01	0.10±0.02	0.6±0.2	0.28±0.02	6.6±0.3

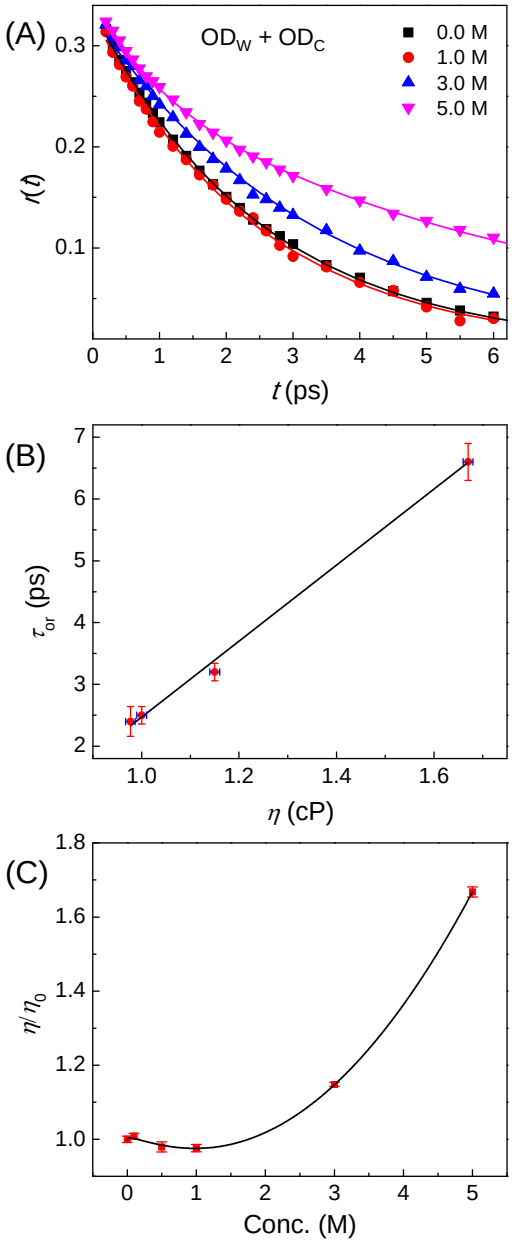

Figure 4. (A) Orientational anisotropy decay, $r(t)$, of the low frequency peak (ODW+ODC) at ~2520 cm^{-1} at different $NaPF_6$ concentrations. (B) Plot of the orientational time constant against the solution viscosity (η). (C) Concentration-dependent viscosity (η/η_0) of aqueous $NaPF_6$ solutions measured at 22 °C. Data points are the values measured by the Oswald viscometer. The line is a fit by the Jones-Dole equation, $\eta/\eta_0 = 1 + A\sqrt{c} + Bc + Dc^2$ with A = 0.0372 M$^{-1/2}$, B = –0.107 M^{-1}, and D = 0.447 M^{-2}.

As opposed to the population decay, the orientational anisotropy decay of HOD measured at the low frequency peak was not well described by the two-state model. In other words, $r(t)$ was not represented by the sum of two contributions of the OD_W and OD_C. The orientational relaxation of water in aqueous solutions is known to be accompanied by the H-bond exchange which is caused by breaking and reforming H-bonds and eventually leads to a global rearrangement of H-bond network. Therefore, the simple two-state model may not be applied to the orientational anisotropy decays of the OD_W and OD_C.

The orientational relaxation of a solute is known to be strongly influenced by the solution viscosity which is a macroscopic property of the solution. The linear relationship between the orientational relaxation time (τ_{or}) and the solution viscosity (η) is given by the Debye-Stokes-Einstein (DSE) equation,[37]

$$\tau_{or} = \frac{\eta V_{eff}}{k_B T} \quad (3)$$

where k_B is the Boltzmann constant and V_{eff} is the effective volume of a rotating solute. In Figure 4(B), the orientational relaxation times (τ_{or}) of HOD in aqueous $NaPF_6$ solutions are plotted against the viscosity (η) of aqueous $NaPF_6$ solutions. In the case of 5.0 M $NaPF_6$ solution, the long time component (τ_{or2}) of the orientational anisotropy decay was used for the plot in Figure 4(B). In Figure 4(B), the orientational relaxation times of HOD are shown to be well correlated with the viscosity of aqueous $NaPF_6$ solutions. In general, the viscosity of aqueous ionic solutions is known to depend on the identity and concentration of the dissolved ions. The concentration-dependent viscosity of aqueous ionic solutions is expressed by the Jones-Dole equation,[38-40]

$$\eta/\eta_0 = 1 + A\sqrt{c} + Bc + Dc^2 \quad (4)$$

where η_0 is the viscosity of neat water, η is the viscosity of aqueous ionic solution, c is the concentration of dissolved ions, and A, B, and D are the Jones-Dole viscosity coefficients depending on the identity of dissolved ions and the solution temperature. The last term in Eq. (4) is not important at a low concentration (i.e., $c < 0.5$ M) but is more useful at higher concentrations. The Jones-Dole A coefficient is related to inter-ionic forces and is always positive. Therefore, the viscosity of aqueous ionic solution tends to increase with the ionic concentration. In contrast, the Jones-Dole B coefficient can be either positive or negative depending on the ion-solvent interactions. The ions with a positive value of B increase the viscosity of the aqueous solutions relative to that for neat water and are classified as structure makers whereas the ions with a negative value of B tend to decrease the solution viscosity and are considered as structure breakers.[10] The Jones-Dole B coefficient for Na^+ and PF_6^- ion is 0.086 and -0.021 mol^{-1}, respectively,[39, 41] and thus Na^+ ion is a structure maker while PF_6^- ion is a structure breaker. In addition, the activation energy for viscous flow at 25 °C is 84 J mol^{-1} for Na^+ ion and -1.09 kJ mol^{-1} for PF_6^- ion.[41] Therefore, Na^+ and PF_6^- ions have opposite effects on the viscosity of aqueous $NaPF_6$ solutions. The concentration-dependent viscosity of aqueous $NaPF_6$ solutions is plotted in Figure 4(C). The viscosity of aqueous $NaPF_6$ solutions shows a nonlinear behavior as a function of $NaPF_6$ concentration and is fit by the Jones-Dole equation in Eq. (4). The Jones-Dole coefficients were obtained to be A = 0.0372 $M^{-1/2}$, B = –0.107 M^{-1}, and D = 0.447 M^{-2}. The Jones-Dole coefficient B for aqueous $NaPF_6$ solution is negative, which indicates that aqueous $NaPF_6$ solution shows a chaotropic behavior as a whole resulting from the fact that PF_6^- ion dominantly contributes to the overall viscosity of aqueous $NaPF_6$ solution.

D. Frequency-dependent transition dipole moment of HOD in aqueous solutions

Figures 5(A) shows Raman spectra measured with aqueous $NaPF_6$ solutions at different $NaPF_6$ concentrations. Similar to the FTIR spectra, the low frequency peak gets blue-shifted and the high frequency peak grows with increasing $NaPF_6$ concentration in Figure 5(A). However, the relative amplitude ratio between the low and high frequency peaks are different in the FTIR and Raman spectra at a given concentration. This result from the fact that the transition dipole moment of the OD stretch vibration varies depending on the H-bond configurations and thus is frequency-dependent (non-Condon effect). The IR absorption and Raman scattering line shapes are commonly expressed as the Fourier transform of a time-dependent correlation function of the dipole operator, μ, and polarizability operator, α, respectively. The IR absorption line shape is obtained from the Fourier transform of the linear response function, which can be written within the semiclassical approximation as[42-44]

$$I_{\mathrm{IR}}(\omega) = \mathrm{Re}\left[\int_{-\infty}^{+\infty} dt e^{i\omega t} \left\langle \mu_{10}(t)\mu_{10}(0)\exp\left[-i\int_0^t d\tau\omega_{10}(\tau)\tau\right]\right\rangle\right] \quad (5)$$

where $\omega_{10}(t)$ is the time-dependent frequency of the υ=0→1 vibrational transition. The IR absorption linear spectrum is proportional to the square of the transition dipole matrix elements, $\mu_{10}(t)$, which is also time-dependent. The measured IR spectrum is related to $I_{\mathrm{IR}}(\omega)$ by

$$S_{\mathrm{IR}}(\omega) \propto \omega\left(1-e^{-\hbar\omega/k_{\mathrm{B}}T}\right) I_{\mathrm{IR}}(\omega) \quad (6)$$

Similarly, the Raman scattering line shape is given by

$$I_{\mathrm{R}}(\omega) = \mathrm{Re}\left[\int_{-\infty}^{+\infty} dt e^{i\omega t} \left\langle \alpha_{10}(t)\alpha_{10}(0)\exp\left[-i\int_0^t d\tau\omega_{10}(\tau)\tau\right]\right\rangle\right] \quad (7)$$

where $\alpha_{10}(t)$ is the time-dependent polarizability operator matrix element. For incoherent Stokes Raman scattering, the observed Raman scattering intensity can be expressed as[45, 46]

$$S_{\mathrm{R}}(\omega) \propto (\omega_{\mathrm{L}} - \omega)^4 \left(1 - e^{-\hbar\omega/k_{\mathrm{B}}T}\right)^{-1} I_{\mathrm{R}}(\omega) \qquad (8)$$

where ω_{L} is the frequency of the excitation source.

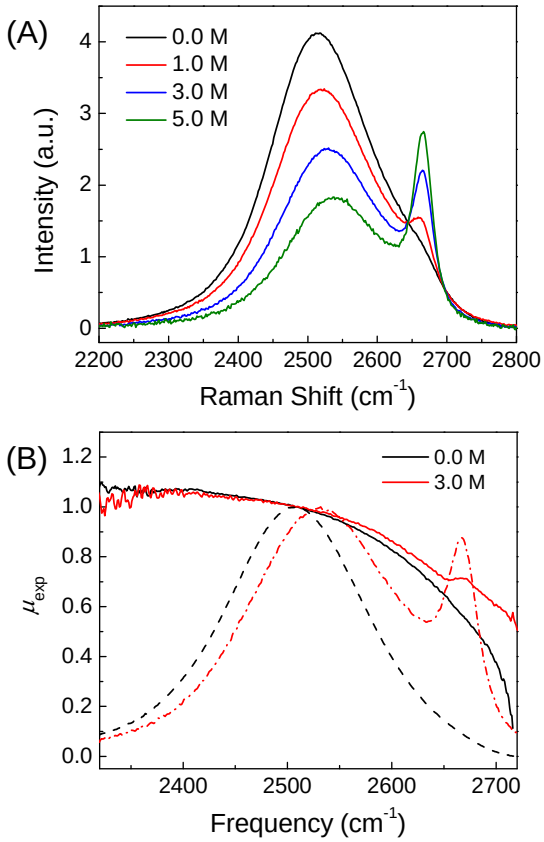

Figure 5. (A) The OD stretch band in the Raman spectra measured with aqueous $NaPF_6$ solutions at different concentrations. (B) Frequency-dependent transition dipole moment of OD stretch band of HOD in neat water and 3.0 M $NaPF_6$ solution. FTIR spectra of 0.0 and 3.0 M are plotted as dashed and dotted-dashed lines, respectively, for comparison.

The frequency-dependent transition dipole moment, $\mu_{\mathrm{exp}}(\omega)$, can be experimentally determined from the ratio of the IR and Raman line shapes. If the transient polarizability is taken to be independent of frequency, it should be possible to obtain the frequency-dependent transition dipole moment without making any assumptions about how it varies with

frequency. Previous experimental and theoretical works indicate that the polarizability only weakly dependent on H-bonding.[47, 48] From Eqs. (6) and (8),

$$\mu_{\exp}(\omega) \propto \sqrt{\frac{I_{\mathrm{IR}}(\omega)}{I_{\mathrm{R}}(\omega)}} = \sqrt{\frac{S_{\mathrm{IR}}(\omega)}{S_{\mathrm{R}}(\omega)} \cdot \frac{\omega}{(\omega_{\mathrm{L}} - \omega)^4}} \left(1 - e^{-\hbar\omega/k_{\mathrm{B}}T}\right) \quad (9)$$

For simplicity, the transition dipole moment of the OD stretch vibration was set to be unity at 2508 cm^{-1} in our calculation and then the relative transition dipole moment was calculated as a function of frequency. Figure 5(B) displays the frequency-dependent transition dipole moment, $\mu_{\exp}(\omega)$, obtained from the IR and Raman spectra measured at 0.0 and 3.0 M. It is clearly seen in Figure 5(B) that the frequency dependence of the transition dipole moment of the OD stretch vibration in neat water and 3.0 M solution is nonlinear and overally the transition dipole moment increases as the OD stretch frequency is decreased. In fact, the frequency-dependent transition dipole moment of OH in neat water was previously investigated by Tokmakoff and coworkers.[44]

As shown in Figure 5(B), $\mu_{\exp}(\omega)$ obtained at 0.0 and 3.0 M becomes significantly different in the high frequency region. At 0.0 M (bulk water), non-H-bonded water molecules appear in the high frequency region while PF_6^-···D–OH configurations are dominant at 3.0 M in the high frequency region. This means that the transition dipole moment of HOD in PF_6^-···D–OH configurations is larger than that of non-H-bonded HOD molecules. This presumably indicates that the details of H-bond configurations (i.e., PF_6^-···D–OH *vs*. non-H-bond) are also important in determining the transition dipole moment of the OD stretch of water in aqueous solutions. In addition to the frequency of the OD stretch, the H-bond acceptor (X) appear to play a role in determining the strength of the transition dipole moment of the OD stretch in HOD···X. It would be interesting to look at how the transition dipole moment of the OD stretch vibration is dependent on the water's local H-bond configurations.

IV. Summary and Concluding Remarks

A detailed study of the concentration-dependent H-bond structure and dynamics of water in aqueous $NaPF_6$ solutions has been presented. The individual dynamics of water in three different subsets in aqueous PF_6^- solutions were investigated here. The experimental approach allowed us to provide more detailed information on the dynamics of water in aqueous ionic solutions. In aqueous $NaPF_6$ solutions, three different subsets of water (OD_W, OD_C, and OD_A) were shown to be well-characterized species in terms of their unique eigen spectra and vibrational lifetimes. As the $NaPF_6$ concentration was increased, the eigen spectra and vibrational lifetimes of OD_W, OD_C, and OD_A remained the same but their amplitudes varied proportionally. On the contrary, the orientational relaxation dynamics of OD_W, OD_C, and OD_A were not able to be separately described. Fayer and coworkers have studied the H-bond structures and dynamics of water in the core-shell reverse micelles.[31] They showed that in the case of the reverse micelles, linear spectrum and population relaxation of water were decomposed into the individual subsets of water in the core and shell of reverse micelles behaving like an observable that depends mainly on the immediate local structure but not on the structural evolution of H-bonds whereas the orientational relaxation was not able to be decomposed into the individual subsets of water in the reverse micelles because it was strongly dependent on the global rearrangement of H-bond network. What they observed in the core-shell reverse micelles is quite similar to our present experimental results observed in aqueous $NaPF_6$ solutions.

In addition, we investigated the frequency-dependent transition dipole moment of the OD stretch vibration of HOD in neat water and 3.0 M $NaPF_6$ solution. The transition dipole moment of the OD stretch vibration was found to be dependent on the hydroxyl stretch

frequency as well as the H-bond acceptors (PF_6^- ion *vs*. non-H-bond). In general, the hydroxyl stretch frequency is sensitively dependent on the local H-bond configurations and the strength of H-bonds. The hydroxyl stretch frequency is more red-shifted when water molecules form the stronger H-bonds with their H-bond acceptors. In a similar way, the relation between the transition dipole moment of the hydroxyl stretch and H-bond strength (or other factors) needs to be further studied in more detail.

As shown here, aqueous PF_6^- solutions are good model systems to study, especially, the dynamics of water in cationic hydration shells in aqueous PF_6^- solutions with different counter cations. The H-bond structures and dynamics of water in different cationic shells (i.e., K^+, Li^+, Mg^{2+}, Ca^{2+}, …) are also interesting to study and will be reported in the future.

Acknowledgements

This work was supported by the National Research Foundation of Korea (NRF) grants funded by the Korea government (MEST) (Nos. 2013R1A1A2009991 and 20100020209) and the KETEP grant (No. 20104010100640). The IR PP experiments were performed in the Multidimensional Spectroscopy Laboratory at Korea Basic Science Institute (KBSI) Seoul Center.

References

1. M. F. Kropman and H. J. Bakker, *Science*, 2001, 291, 2118-2120.
2. D. Laage and J. T. Hynes, *Proc. Nat. Acad. Sci. USA*, 2007, 104, 11167-11172.
3. S. Park and M. D. Fayer, *Proc. Natl. Acad. Sci. USA*, 2007, 104, 16731-16738.
4. S. Park, D. E. Moilanen and M. D. Fayer, *J. Phys. Chem. B*, 2008, 102, 5279-5290.
5. S. Park, M. Odelius and K. J. Gaffney, *J. Phys. Chem. B.*, 2009, 113, 7825-7835
6. R. Costard, N. E. Levinger, E. T. Nibbering and T. Elsaesser, *J. Phys. Chem. B*, 2012, 116, 5752-5759.
7. H. Kim, S. Park and M. Cho, *Phys. Chem. Chem. Phys.*, 2012, 14, 6233-6240.
8. C. H. Giammanco, D. B. Wong and M. D. Fayer, *J. Phys. Chem. B*, 2012, 116, 13781-13792.
9. S. T. van der Post and H. J. Bakker, *J. Phys. Chem. B*, 2014, 118, 8179-8189.
10. Y. Marcus, *Chem. Rev.*, 2009, 109, 1346-1370.
11. N. E. Levinger, *Curr. Opin. Colloid. Interface Sci.*, 2000, 5, 118-124.
12. Q. Zhong, A. Baronavski and J. Owrutsky, *J. Chem. Phys.*, 2003, 118, 7074.
13. I. R. Piletic, H.-S. Tan and M. D. Fayer, *J. Phys. Chem. B*, 2005, 109, 21273-21284.
14. B. Baruah, J. M. Roden, M. Sedgwick, N. M. Correa, D. C. Crans and N. E. Levinger, *J. Am. Chem. Soc.*, 2006, 128, 12758-12765.
15. R. Costard, N. E. Levinger, E. T. J. Nibbering and T. Elsaesser, *J. Phys. Chem. B*, 2012, 116, 5752-5759.
16. V. Etacheri, R. Marom, R. Elazari, G. Salitra and D. Aurbach, *Energy Environ. Sci.*, 2011, 4, 3243-3262.
17. Z. Zeng, W.-I. Liang, H.-G. Liao, H. L. Xin, Y.-H. Chu and H. Zheng, *Nano Lett.*, 2014, 14, 1745-1750.
18. U. Schroder, J. D. Wadhawan, R. G. Compton, F. Marken, P. A. Z. Suarez, C. S.

Consorti, R. F. d. Souzab and J. Dupont, *New J. Chem.*, 2000, 24, 1009-1015.

19. A. Triolo, A. Mandanici, O. Russina, V. Rodriguez-Mora, M. Cutroni, C. Hardacre, M. Nieuwenhuyzen, H.-J. Bleif, L. Keller and M. A. Ramos, *J. Phys. Chem. B*, 2006, 110, 21357-21364.
20. C. S. S. a. S. B. Cesar Aliaga, *Phys. Chem. Chem. Phys.*, 2007, 9, 3683-3700.
21. P. Hapiot and C. Lagrost, *Chem. Rev.*, 2008, 108, 2238-2264.
22. G. E. Walrafen, *J. Chem. Phys.*, 1971, 55, 768-792.
23. O. Kristiansson, J. Lindgren and J. d. Villepin, *J. Phys. Chem.*, 1988, 92, 2680-2685.
24. M. Śmiechowski, E. Gojło and J. Stangret, *J. Phys. Chem. B*, 2004, 108, 15938-15943.
25. H. Son, D. Nam and S. Park, *J. Phys. Chem. B*, 2013, 117, 13604-13613.
26. D. Nam, C. Lee and S. Park, *Phys. Chem. Chem. Phys.*, 2014, 16, 21747-21754
27. K.-K. Lee, K.-H. Park, D. Kwon, J.-H. Choi, H. Son, S. Park and M. Cho, *J. Chem. Phys.*, 2011, 134, 064506.
28. H. Son, J. Haneul, S. R. Choi, H. W. Jung and S. Park, *J. Phys. Chem. B*, 2012, 116, 9152-9159.
29. M. J. Frisch, G. W. Trucks, H. B. Schlegel, G. E. Scuseria, M. A. Robb, J. R. Cheeseman, J. A. Montgomery, Jr. , T. Vreven, K. N. Kudin, J. C. Burant, J. M. Millam, S. S. Iyengar, J. Tomasi, V. Barone, B. Mennucci, M. Cossi, G. Scalmani, N. Rega, G. A. Petersson, H. Nakatsuji, M. Hada, M. Ehara, K. Toyota, R. Fukuda, J. Hasegawa, M. Ishida, T. Nakajima, Y. Honda, O. Kitao, H. Nakai, M. Klene, X. Li, J. E. Knox, H. P. Hratchian, J. B. Cross, V. Bakken, C. Adamo, J. Jaramillo, R. Gomperts, R. E. Stratmann, O. Yazyev, A. J. Austin, R. Cammi, C. Pomelli, J. W. Ochterski, P. Y. Ayala, K. Morokuma, G. A. Voth, P. Salvador, J. J. Dannenberg, V. G. Zakrzewski, S. Dapprich, A. D. Daniels, M. C. Strain, O. Farkas, D. K. Malick, A. D. Rabuck, K. Raghavachari, J. B. Foresman, J. V. Ortiz, Q. Cui, A. G. Baboul, S. Clifford, J.

Cioslowski, B. B. Stefanov, G. Liu, A. Liashenko, P. Piskorz, I. Komaromi, R. L. Martin, D. J. Fox, T. Keith, M. A. Al-Laham, C. Y. Peng, A. Nanayakkara, M. Challacombe, P. M. W. Gill, B. Johnson, W. Chen, M. W. Wong, C. Gonzalez and J. A. Pople, Gaussian, Inc., Wallingford, CT, *Gaussian 09*, Rev. C. 01 edn., 2012.

30. I. M. Alecu, J. Zheng, Y. Zhao and D. G. Truhlar, *J. Chem. Theory Comput.* , 2010, 6, 2872-2887.
31. I. Piletic, D. E. Moilanen, D. B. Spry, N. E. Levinger and M. D. Fayer, *J. Phys. Chem. A*, 2006, 110, 4985-4999.
32. Y. L. A. Rezus and H. J. Bakker, *J. Chem. Phys.*, 2006, 125, 144512.
33. Y. Marcus, *Ion Solvation*, Wiley, New York, 1985.
34. K. J. Tielrooij, N. Garcia-Araez, M. Bonn and H. J. Bakker, *Science*, 2010, 328, 1006-1009.
35. K. Kinosita, A. Ikegami and S. Kawato, *Biophys. J.*, 1982, 37, 461-464.
36. K. J. Gaffney, I. R. Piletic and M. D. Fayer, *J. Chem. Phys.*, 2003, 118, 2270-2278.
37. H. Son, Y. Kwon, J. Kim and S. Park, *J. Phys. Chem. B* 2013, 117, 2748−2756.
38. G. Jones and M. Dole, *J. Am. Chem. Soc.*, 1929, 51, 2950−2964.
39. H. D. B. Jenkins and Y. Marcus, *Chem. Rev.*, 1995, 95, 2695-2724.
40. Y. R. Dougassa, J. Jacquemin, L. E. Ouatani, C. Tessier and M. m. Anouti, *J. Phys. Chem. B*, 2014, 118, 3973−3980.
41. E. R. Nightingale, in *Chemical Physics of Ionic Solutions*, eds. B. E. Conway and R. G. Barradas, Wiley, New York, 1966, ch. 7, pp. 87-100.
42. S. Mukamel, *Principles of Nonlinear Optical Spectroscopy*, Oxford University Press, New York, 1995.
43. J. R. Schmidt, S. A. Corcelli and J. L. Skinner, *J. Chem. Phys.*, 2005, 123, 044513(044513).

44. J. J. Loparo, S. T. Roberts, R. A. Nicodemus and A. Tokmakoff, *Chem. Phys.*, 2007, 341, 218-229.

45. D. A. McQuarrie, *Statistical Mechanics*, Haprer and Row, New York, 1976.

46. G. E. Walrafen, M. R. Fisher, M. S. Hokmabadi and W. H. Yang, *J. Chem. Phys.*, 1986, 85, 6970.

47. Y. Y. Efimov and Y. I. Naberukhin, *Faraday Discuss, Chem. Soc.*, 1988, 85, 117-123.

48. S. A. Corcelli and J. L. Skinner, *J. Phys. Chem. A*, 2005, 109, 6154-6165.

TOC graphic

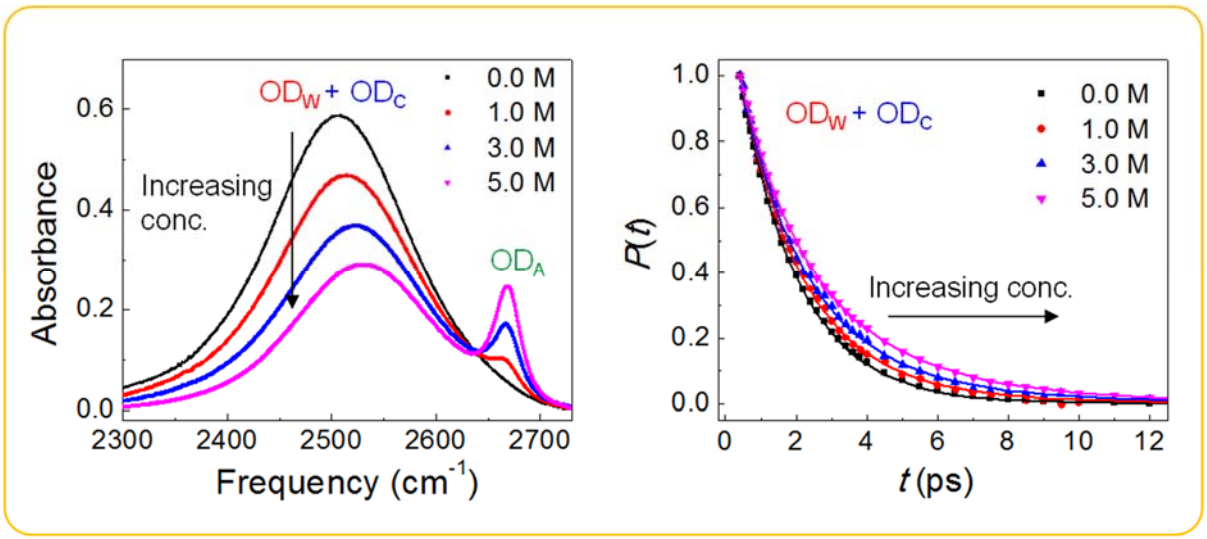

The H-bond structures and dynamics of water in bulk and ionic hydration shells in aqueous $NaPF_6$ solutions were measured at different $NaPF_6$ concentrations.